JGR Atmospheres

RESEARCH ARTICLE
10.1029/2018JD029346

Dependence of Vertical Alignment of Cloud and Precipitation Properties on Their Effective Fall Speeds

Mikhail Ovchinnikov[1], Scott Giangrande[2], Vincent E. Larson[3], Alain Protat[4], and Christopher R. Williams[5]

[1]Pacific Northwest National Laboratory, Richland, WA, USA, [2]Brookhaven National Laboratory, Upton, NY, USA, [3]Department of Mathematical Sciences, University of Wisconsin–Milwaukee, Milwaukee, WI, USA, [4]Centre for Australian Weather and Climate Research, Melbourne, Victoria, Australia, [5]Earth System Research Laboratory, NOAA, Boulder, CO, USA

Abstract The vertical structure of clouds unresolved in large-scale weather prediction and climate models is controlled by an overlap assumption. When a binary representation (cloud or no cloud) of subgrid horizontal variability is replaced by a probability density function (PDF) treatment of cloud-related variables, a cloud occurrence overlap needs to be replaced by a PDF overlap. The PDF overlap can be quantified by a correlation length scale, z_0, indicating how rapidly rank correlation of distributions at two levels diminishes with increasing level separation. In this study, we show that z_0 varies widely for different properties (e.g., number and mass mixing ratios) and different hydrometeor types (cloud liquid and ice, rain, snow, and graupel) and that corresponding fall speed, V_f, is the primary factor controlling the degree of their vertical alignment, with vertical shear of the horizontal wind playing a smaller role. Linear and power law parametric relationships between z_0 and V_f are derived using cloud-resolving simulations of convection under midlatitude continental and tropical oceanic conditions, as well as observations from vertically pointing dual-frequency radar profilers near Darwin, Australia. The functional form of z_0-V_f relationship is further examined using simple conceptual models that link variability in horizontal and vertical directions and provide insights into the role of V_f and wind shear. Being based on a physical property (i.e., fall speed) of hydrometeors rather than artificially defined and model-specific hydrometeor types, the proposed parameterization of vertical PDF overlap can be applied to a wide range of microphysics treatments in regional and global models.

Key Points:
- Rank correlations of cloud and precipitation distributions at adjacent levels are computed for model-simulated and radar-observed fields
- Correlation length scale, or PDF overlap, is a function of mean fall speed of considered property
- Wind shear reduces alignment of slow falling species, but has limited effect on faster precipitating hydrometeor categories

Supporting Information:
- Supporting Information S1

Correspondence to:
M. Ovchinnikov,
mikhail@pnnl.gov

Citation:
Ovchinnikov, M., Giangrande, S., Larson, V. E., Protat, A., & Williams, C. R. (2019). Dependence of vertical alignment of cloud and precipitation properties on their effective fall speeds. *Journal of Geophysical Research: Atmospheres*, *124*, 2079–2093. https://doi.org/10.1029/2018JD029346

Received 16 JUL 2018
Accepted 11 JAN 2019
Accepted article online 28 JAN 2019
Published online 18 FEB 2019

1. Introduction

Growing sophistication of microphysics representations in regional and global atmospheric models combined with the desire for a more uniform treatment of spatial variability across different model components has spurred several recent attempts to improve parameterization of vertical alignment of cloud and precipitation properties on subgrid scales. A common approach consists of drawing a number of profiles, known as subcolumns, which collectively represent predicted horizontal variability at each model level, while at the same time ensuring the desired correlation of sampled variables in the vertical. The approach represents an extension of a traditional cloud overlap assumption (also called cloud fraction overlap or cloud occurrence overlap), used to describe the probability of presence or absence of a cloud at two levels in a column, to a situation where a given property varies (horizontally) inside the cloud. When the binary representation (cloud or no-cloud) of horizontal variability is replaced by a probability density function (PDF) of cloud or precipitation variables, cloud occurrence overlap is replaced by a PDF overlap (e.g., Larson, 2007; Pincus et al., 2005).

Vertical PDF overlap treatment and resulting subcolumns can impact computations of radiative transfer (e.g., Barker, 2008; Oreopoulos et al., 2004; Paquin-Ricard et al., 2016; Wang, 2017), output from simulators for active or passive surface- or satellite-based remote sensors (e.g., Bodas-Salcedo et al., 2011; Hillman et al., 2018), or modeled effects of precipitation on thermodynamics and microphysics (e.g., Griffin & L, 2016). Although in many cases corresponding model components use their own task-specific subcolumn generators, it is desirable to employ a consistent overlap treatment throughout the model. Previous studies have examined vertical alignment of various cloud properties, including radar-retrieved cirrus ice water

content (Hogan & Illingworth, 2003), model-generated total (vapor + cloud liquid and ice) water content (Pincus et al., 2005), and cloud (liquid + ice) water content (Raisanen et al., 2004; Wang, 2017). Ovchinnikov et al. (2016) used a cloud-resolving model to examine the vertical PDF overlap of 10 microphysical variables. that is, number and mass mixing ratios for five hydrometeor types: cloud liquid, rain, cloud ice, snow, and graupel. They found that the PDF overlap varies widely between these categories and hypothesized that these variations might be attributable to differences in fall speed of these hydrometeors.

The goal of this study is twofold. First, we seek to quantify the dependency of the PDF overlap on hydrometeor fall speed, which was noted by Ovchinnikov et al. (2016) in their analysis of simulated cloud fields. Second, we aim to provide corroborating observational evidence for this dependency from ground-based profiling radars. The rest of the paper is organized as follows. Section 2 describes the model output and observational data set used in the analysis and outlines the method for quantifying PDF overlap using a correlation length scale. Results of the analysis, including parametric expression relating correlation length scale and fall speed, are presented in section 3. Section 4 provides further discussion of the found relationship between vertical correlation length scale and fall speed and the role of wind shear. Finally, the main findings are summarized in section 5.

2. Approach

2.1. Model Configuration and Simulations

Model simulations of midlatitude continental and tropical oceanic convection analyzed in this paper are taken from Wong and Ovchinnikov (2017). A cloud-resolving model called System for Atmospheric Modeling, or SAM (version 6.10.6, Khairoutdinov & Randall, 2003), is used to simulate two Intensive Observation Periods conducted by the U.S. Department of Energy Atmospheric Radiation Measurement Climate Research Facility over Southern Great Plains (SGP) in north central Oklahoma in June of 1997 (Xu et al., 2002) and near Darwin, Australia, in January of 2006 (the Tropical Warm Pool International Cloud Experiment, or TWP-ICE; May et al., 2008). The simulations, hereafter referred to as SGP and TWP, respectively, use forcing data sets, including initial soundings, surface sensible and latent heat fluxes, and large-scale advection tendencies for temperature and moisture, which are available through Atmospheric Radiation Measurement data archive (http://archive.arm.gov). The model is run on a horizontally uniform rectangular grid with 1-km spacing in a 128×128 km^2 domain and a stretched 128-level vertical grid with grid spacing increasing from 55 m near the surface to 250 m above 6 km. The model top is set at 27.75 km. The lateral boundaries are periodic in both horizontal directions. The model time steps are 5 s for SGP and 6 s for TWP simulation, respectively. The slightly shortened time step for SGP reflects stricter computational stability requirements for modeling more intense vertical motions in continental compared to the maritime convection. Further datails on the model setup can be found in Wong et al. (2015) and Wong and Ovchinnikov (2017).

The SGP simulation is run for a 4-day period from 27 June to 1 July 1997 and TWP simulation is run for 3.5-day period from 12 UTC 21 January to 0 UTC 25 January 2006. Unlike Ovchinnikov et al. (2016), where only selected day-long periods were examined, here we analyze the whole multi-day simulations and, therefore, include a wider range of cloudy conditions. In both simulations, instantaneous three-dimensional snapshots of model variables are archived at 10-min intervals.

The model employs a two-moment microphysics scheme that predicts mass and number mixing ratios for cloud liquid and ice, rain, snow, and graupel (Morrison et al., 2005, 2009). Each snapshot provides two-dimensional spatial distributions of these variables at each model level and the vertical coherence of these distributions, or PDF overlap, between adjacent levels is then quantified using a rank correlation coefficient R, as described in more detail later in this section. Grid cells containing mass mixing ratios larger than 10^{-4} g/kg and number mixing ratios larger than 10^3 kg^{-1} for cloud droplets and 1 kg^{-1} for rain droplet and ice particles are included in the analysis. Sensitivity tests indicate that increasing these thresholds by an order of magnitude has only a minor effect on the presented results.

Figures 1–3 illustrate the time evolution of mean profiles of in-precipitation rain, snow, and graupel mass mixing ratios, fractional area coverage, and mass-weighted fall speeds for the two simulations. The SGP simulation includes three separate periods of strong convective activity. In the first two periods, the

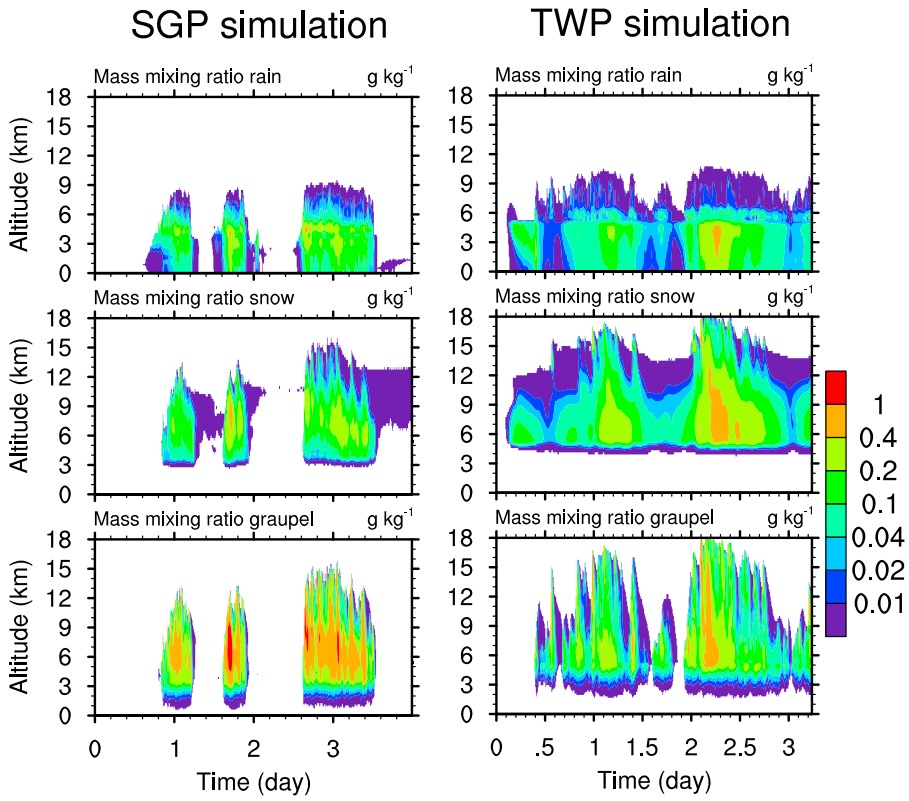

Figure 1. Time evolution of horizontally averaged in-precipitation mass mixing ratio profiles for rain (top), snow (middle), and graupel (bottom) from Southern Great Plains (SGP, left column) and Tropical Warm Pool (TWP, right column) simulations.

fractional area of precipitation reaches about 0.2 (Figure 2), suggesting that they are dominated by isolated convective cells. The third and strongest event includes a period of extended stratiform precipitation, evident from precipitation area fraction above 0.6. In the simulation of moister TWP environment, precipitation occurs through much of the domain after the first few spin-up hours, with area fraction of snow above and rain below the melting level averaging near 0.9 (Figure 2). Stratiform precipitation dominates this simulation, but several periods of enhanced deep convection are evident and correspond to increased rain and graupel area fraction above the freezing level. The in-precipitation mean mass mixing ratios, that is, values horizontally averaged over grid points with corresponding mass mixing ratios larger than 10^{-4} g/kg, for the three hydrometeor categories are comparable and in the range of a few tenths of a gram per kilogram (Figure 1). Mass-weighted fall speeds for the three shown types of hydrometeors are markedly different (Figure 3). Snow is falling with the slowest speed from a narrow range (1–2 m/s), rain fall speed is the fastest (4–6 m/s), and graupel fall speed is in-between these two categories (2–4 m/s).

2.2. Radar Observations

This study uses an extended data set from two wind profilers operated at 50- and 920-MHz frequencies near Darwin, Australia, during the 2005–2006 monsoon season, which includes the TWP-ICE period. The data set is described by Kumar et al. (2015), who used it to analyze mass flux characteristics of tropical cumulus clouds, and by Schumacher et al. (2015), who documented vertical motion statistics segregated by cloud type. This study relies on vertical air motions retrieved from Doppler spectra from the two profilers using an algorithm by Williams (2012), which avoids making assumptions on hydrometeor fall speeds needed for a single profiler retrieval (e.g., Giangrande et al., 2016) or mass continuity assumptions used in multi-Doppler retrievals (e.g., North et al., 2017).

Following Protat and Williams (2011), a bulk radar reflectivity-weighted hydrometeor fall speed is found as a residual of the retrieved vertical air motions and measured mean Doppler velocity of precipitating

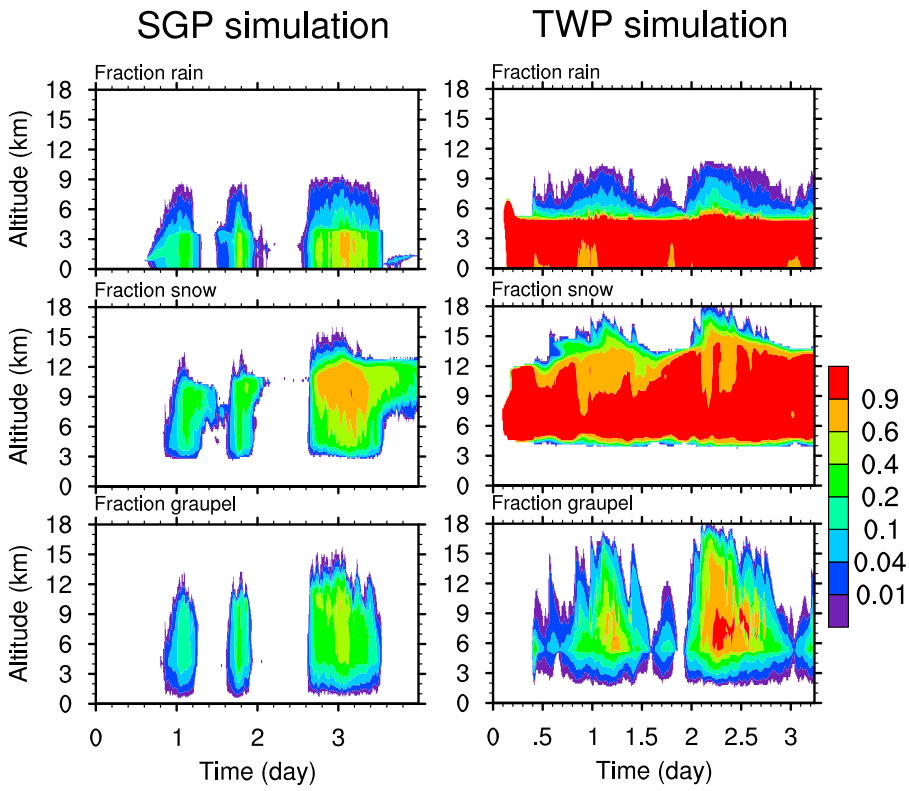

Figure 2. Same as Figure 1 but for profiles of fractional area cover.

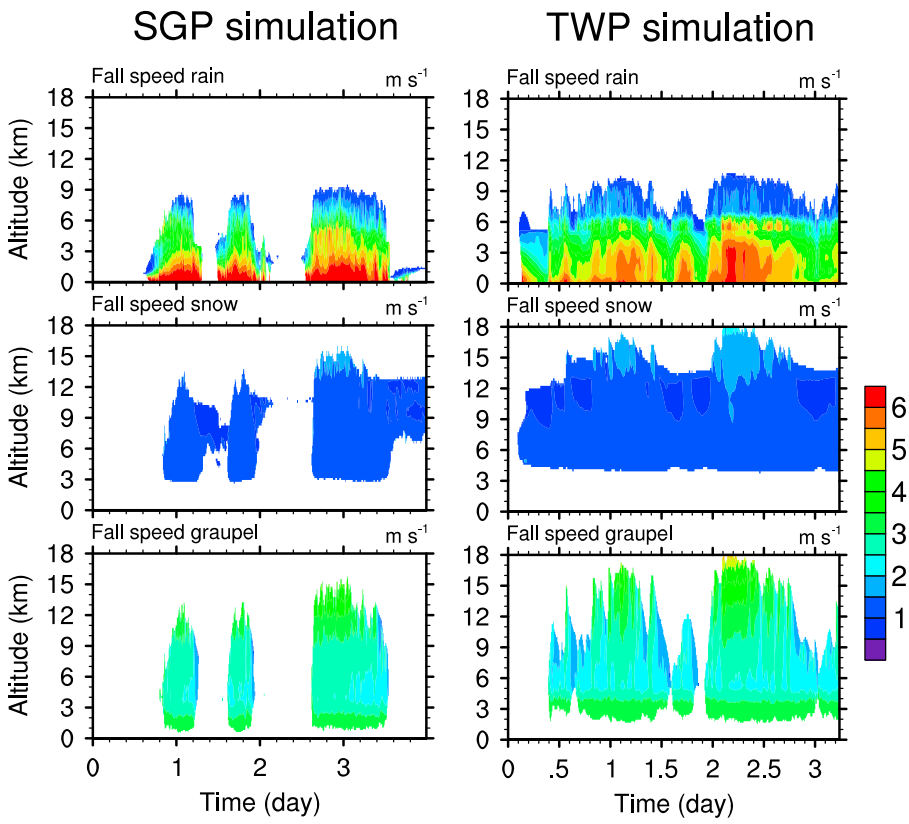

Figure 3. Same as Figure 1, but for profiles of mass-weighted hydrometeor fall speeds.

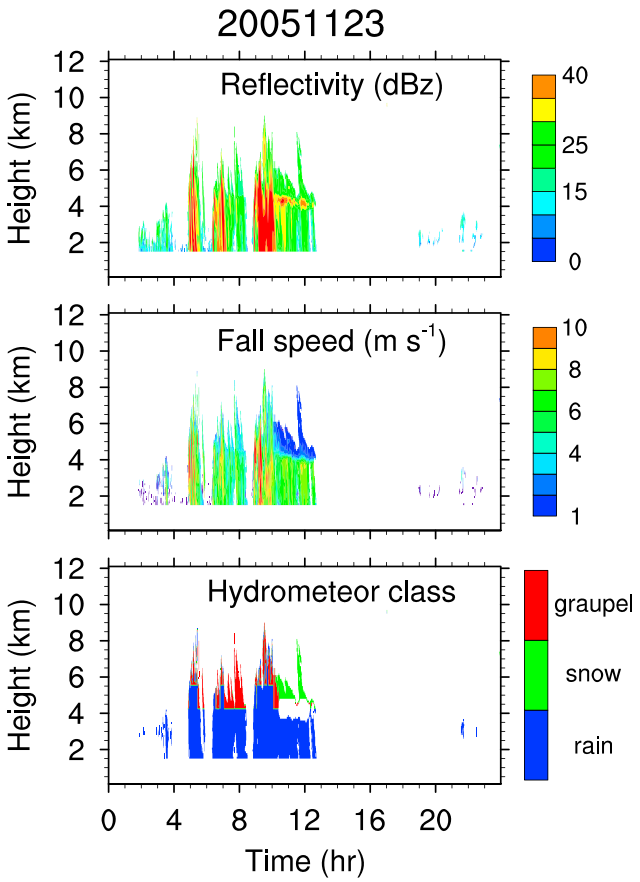

Figure 4. Radar reflectivity from the 920-MHz wind profiler (top), retrieved reflectivity weighted fall speed (middle), and predominant hydrometeor class (bottom) observed on 23 November 2005.

hydrometeors. Vertical velocity of air and, therefore, fall speeds are not retrieved below 1.7 km, which is the lowest sampled range of the 50-MHz profiler (Williams, 2012), and those levels are excluded from the present analysis.

Observed radar reflectivity factors, which are proportional to higher-order moments of hydrometeor size distributions than number and mass concentrations discussed earlier, and corresponding reflectivity-weighted fall speeds are used here for analysis of PDF overlap. Observations from a zenith pointing profiler provide a height-time curtain view of the atmosphere. PDFs of observed or retrieved variables at each level are then obtained from time series at that level. These PDFs, and consequently PDF overlap characteristics, are representative of a certain time period or convective event. In the presented study, each observational PDF is derived from day-long time series.

In the presented analysis, radar reflectivities and fall speeds from the entire data set are grouped into three subsets based on determined dominant hydrometeor class. A fuzzy-logic echo classification (Giangrande et al., 2013, 2016) has been implemented to differentiate between convective, periphery convective, and stratiform precipitation regions and to identify possible radar artifacts and nonmeteorological returns. This echo classification is then combined with observed reflectivity and retrieved fall speed to assign one of three hydrometeor classes (rain, snow, and graupel) to each time-altitude sample.

Although we refer to rain, snow, and graupel classes or hydrometeor categories in discussing both model and observational results, the following distinctions must be noted. Because only one type is identified for each sample volume in radar observations, it should be considered as a predominant type. Hydrometeors of other types are likely to be present at the same altitude at the same time, but the identified type is assumed to contribute the most to the radar signal. In model simulations, on the other hand, when a mixture of different hydrometeor types is present in a grid cell, each type contributes to its own PDF regardless of its relative amount in that mixture. One consequence of this sampling difference is a larger fractional cover for each hydrometeor type and larger numbers of samples for their respective distributions in simulations compared to observations. We also note that in the presented hydrometeor classification, there is no separate category for hail, although the deepest and strongest convective cores in the observational data set are likely to contain large high-density ice particles, such as frozen rain drops or small hail. For these particles to be called a dominant type, however, the core reflectivity would have to be above 50–55 dBZ. Such high reflectivities occur only rarely in our data set.

Figure 4 illustrates the time evolution of profiles of radar reflectivity factor and retrieved hydrometeor fall speed and type for one convective event observed on 23 November 2005. A series of progressively stronger convective clouds passes over the profilers between hours 2 and 10, followed by trailing stratiform clouds lasting until 13 hr. Isolated shallower convective clouds are also observed during the last 5 hr of this 24-hr period. Stronger convection is characterized by higher cloud tops, as well as higher reflectivity and faster fall speeds. The hydrometeor classification algorithm identifies that the radar return comes primarily from rain in the lower part of the convection and rimed ice particles, or graupel, in the upper part. In downdrafts and weak updrafts, the rain-graupel boundary is located at or near the melting level, but in strong updrafts it shifts to higher altitude. In stratiform regions, frozen hydrometeors are classified as snow. Bright band regions are excluded from consideration by the current classification algorithm and masked out in Figure 4.

Figure 5 shows the Doppler velocity from the 920-MHz radar and air velocity retrieved from 50-MHz profiler for the same day, from which the fall speed of hydrometeors shown in Figure 4 are deduced. While the 920-MHz Doppler velocity often provides a good estimate of the fall speed, air motion contribution is significant at times. For example, a peak of Doppler velocity between 2 and 3 km at 7 hr (Figure 5, top panel) is in a

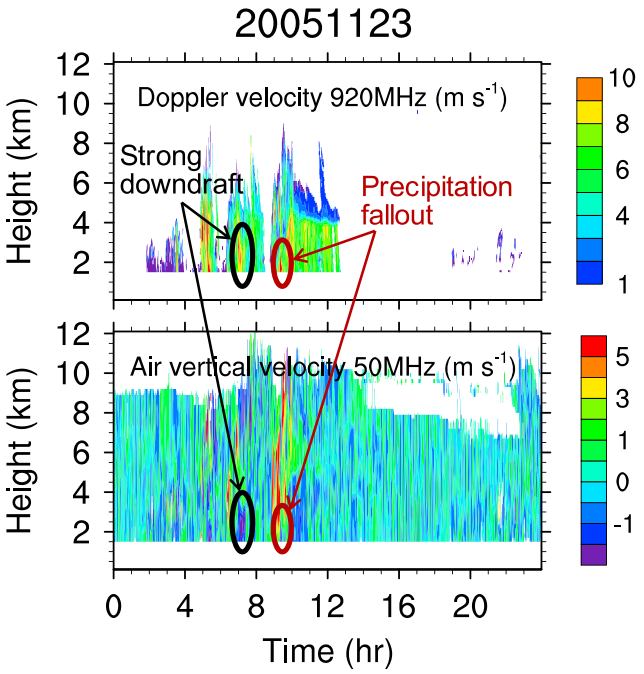

Figure 5. Doppler velocity (positive downward) as measured by the 920-MHz wind profiler (top) and vertical velocity of air (positive upward) retrieved from the 50-MHz profiler (bottom) on 23 November 2005. The sum of the two gives reflectivity weighted hydrometeor fall speed shown in the middle panel of Figure 4. Two regions of high Doppler velocities from 920-MHz profiler are indicated, one dominated by strong downward air motions and another due to precipitation (rain) fall speed.

region of significant downdraft (Figure 5, bottom panel) and therefore does not translate into higher fall speed values at this location (Figure 4, middle panel). Comparable Doppler velocities at similar altitudes 2 hr later, on the other hand, are in a region of updrafts or weak downdrafts and, therefore, are caused primarily by precipitation fallout, which is reflected in high retrieved fall speeds. This highlights the benefits of using dual wavelength profilers to retrieve hydrometeor fall speeds in this study.

2.3. PDF Overlap

Following Ovchinnikov et al. (2016), the vertical PDF overlap, or alignment, is characterized in this study by computing rank correlation (R; or Spearman correlation coefficient) between distributions of variables at two levels separated by Δz. $R = 1$ defines maximum (perfect) overlap and $R = 0$ corresponds to random PDF overlap (Ovchinnikov et al., 2016). Only overlapping parts of distributions are accounted for, that is, only profiles that include nonzero values at both considered levels are included in computation of ranking and correlation coefficient. Hence, at any level, different subsets of points may be used for computing correlation of this level with levels above and below. Because points voided of hydrometeors are excluded, the resulting correlation is not directly dependent on cloud or precipitation fraction. Note that it would be problematic to include the condensate-free areas in this type of correlation because multiple zero values cannot be unambiguously ranked. These zeros can be incorporated into the Pearson-type correlation between actual physical variables rather than their ranks, although doing so would require taking special care to mitigate the effect of cloud fraction, or the outer scale, that is, the size of cloud-free area outside the convection region included in the analysis (Marchand, 2012). Using rank correlation instead of Pearson correlation also removes the dependency of R on the shape of the distribution —for example, its variance, or skewness—and makes it less sensitive to outliers or rare extreme values, which often strongly impact the Pearson correlation coefficient. It is also worth noting that since the (spatial) correlation is computed for rank distributions where ranking is done independently for each level, the overlap (or correlation) does not directly depend on the vertical gradient of absolute values of the considered variables. For example, evaporation can reduce the mass mixing ratio of rain drops below cloud base but does not reduce vertical PDF correlation if the evaporation reduces rain mixing ratio proportionately at every point in a horizontal layer. Evaporation reduces the vertical PDF correlation only if it switches the ranking of rain mixing ratios in two or more columns, which might occur if evaporation is horizontally inhomogeneous, as will be discussed further in section 4.

Because interlayer correlation is a function of layer separation distance Δz, we convert R into a correlation length scale z_0 by inverting

$$R = \exp(-\Delta z / z_0) \quad (1)$$

and use z_0 as a measure of PDF overlap (e.g., Hogan & Illingworth, 2003; Pincus et al., 2005). Previous studies found that caution must be applied in using a simple functional form of decorrelation length scale (for cloud occurrence) over a broad range of separation distances (e.g., Neggers et al., 2011). Our analysis, however, is confined to a narrow Δz range, from 100 to 250 m, where different functional forms can provide comparable fits to the R-Δz relationship. The broader validity of inverse exponential reduction of PDF correlation with Δz must be examined in the future.

3. Results

3.1. Radar Observations

A total of 54 convective events, or days with convection, are analyzed here. Time-height distributions of radar reflectivity factor and retrieved hydrometeor fall speed and predominant type for all events are

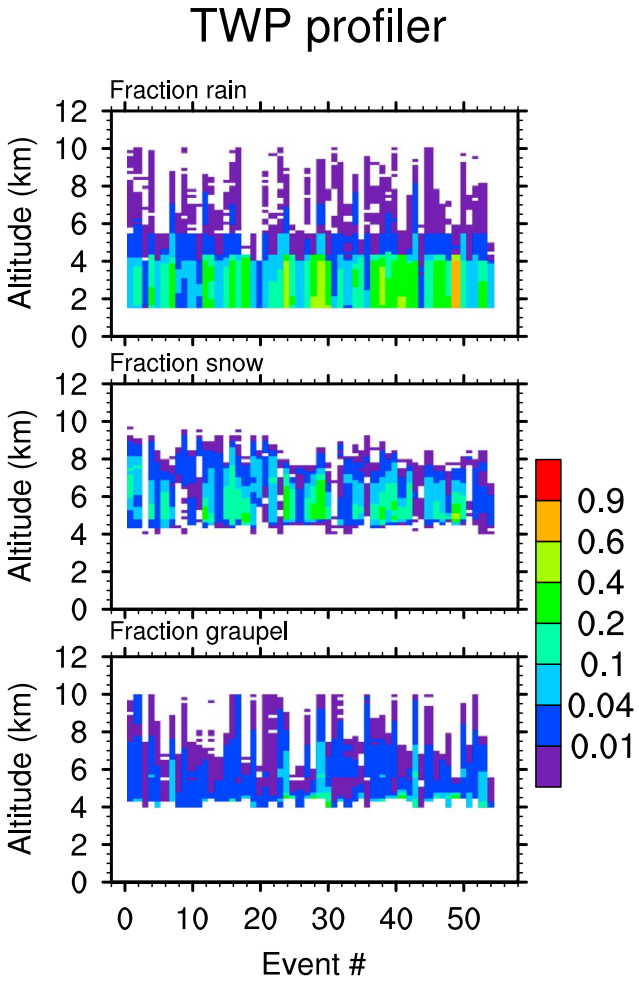

Figure 6. Profiles of frequency of occurrence of radar-observed hydrometeors at all altitudes for 54 events. Panels from top to bottom are for rain, snow, and graupel separately. Hydrometeor classification is not performed below 1.7 km (see text for details). TWP = Tropical Warm Pool.

shown in the supporting information (Figures S1–S3). Figure 6 illustrates that cloud and precipitation fraction varies widely over these days, from a few hundredths to 0.6. Here fraction refers to fraction of time when hydrometeors are present at a given level and is equivalent to the frequency of occurrence on that day. The mean fraction is 0.2–0.25 below 4.5 km, which is an approximate altitude of the melting level, and decreases with altitude rapidly above that level. Unlike the fractional cover from simulations shown in Figure 2, fraction presented here is a function of not only the size of the observed convective system but also its position relative to the profilers that provide a zenith pointing beam view.

Below the melting level the precipitation fraction is attributed almost exclusively to rain. Above the melting level, the most frequent precipitation type is snow, followed by graupel, and, occasionally, rain. Most of the events have at least some rain above the melting level, although its frequency is an order of magnitude lower than below the melting level. The microphysical properties of rain above the melting level also have much greater spatial and temporal variability, as evident by the profiles of the mean fall speed (Figure 7). Both high (larger than 10 m/s) and low (less than 6 m/s) fall speeds are found often above 5 km, but rarely below. This is likely due to differences in both sampling and physics of rain formation. Above the melting level, rain is associated with relatively narrow convective towers, and its properties change rapidly in space and time, so profiles from a narrow column sampled above the radar may deviate significantly from a mean profile over a broader area. In addition, rain above the melting layer is either transported there by strong updrafts or formed primarily through collision-coalescence of droplets. Both processes are most efficient during relatively short periods of active convection development, which may explain intermittency in rain properties at these altitudes, while rain below the melting level comes predominantly from melting snow in more widely spread and steadier stratiform clouds. Finally, fast fall speeds in the strongest convective cores above the melting level may be in part due to presence of frozen drops and/or hail.

In the layer between 5 and 8 km, snow is the dominant species in terms of frequency of occurrence (Figure 6). This hydrometeor category is most commonly associated with regions of stratiform precipitation, which last longer and have greater horizontal extent than regions of intense convection. In stronger convection, graupel or heavily rimed particles are identified more often above the melting level. Conditions for graupel formation are similar to those leading to rain above the melting level, since both require presence of significant cloud water for riming or collisional growth of graupel or rain, respectively. Consequently, profiles dominated at higher altitudes by graupel are often intermixed with those dominated by rain (Figures 4 and S3).

As noted above, the variability of reflectivity weighted fall speed for rain is large near and above the melting level. Below the melting level, where rain is much more prevalent, the mean fall speed of rain is more uniform and is typically in the 6–10 m/s range, with an ensemble mean between 7 and 9 m/s depending on the altitude. The reflectivity weighted fall speed of graupel is slightly lower, with a mean of 6–7 m/s, while the reflectivity of snow has the slowest effective fall speed between 1 and 2 m/s, which is nearly constant with height. In interpreting the retrieved fall speed values, it is important to keep in mind that although they are assigned to a predominant hydrometeor category, they include contributions from other particle types. Presence of graupel or rain in snow-dominated pixels, for example, will introduce a high bias in retrieved snow fall speeds, while retrieved rain fall speeds can be biased low when snow and graupel are present.

Inverse exponential length scale z_0 for ranked correlation coefficients computed for PDFs of radar reflectivity factors at two adjacent levels is shown in Figure 8. Note that for levels that are 100 m apart, as they are in

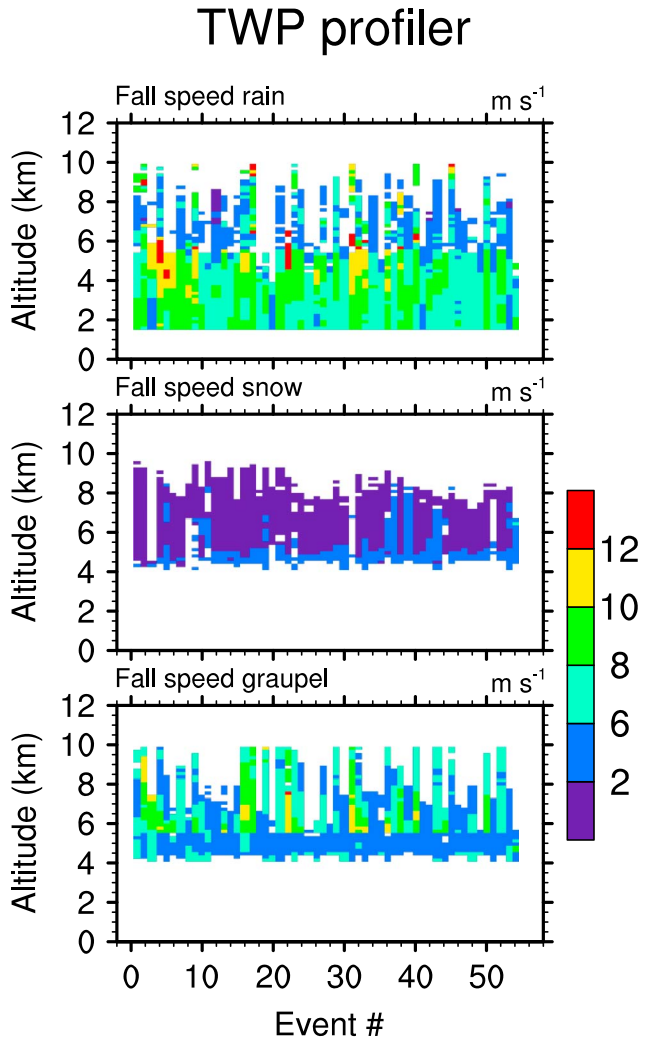

Figure 7. Profiles of radar-retrieved hydrometeor fall speed for 54 events. Panels from top to bottom are for rain, snow, and graupel separately. Fall speed retrievals are not available below 1.7 km. TWP = Tropical Warm Pool.

the analyzed radar profiler data sets, z_0 of 10, 1, and 0.1 km correspond to rank correlation coefficients of 0.99, 0.90, and 0.37, respectively. It is important to keep in mind that the correlation length scale computed from distributions at layers in close proximity to each other only shows how correlated these distributions are and does not contain information about actual vertical extent of coherent structures. Thus, it is not surprising that although there are few, if any, clouds in the presented analysis that are over 10-km deep, values of z_0 in excess of 10 km are common. For example, the correlation length scale for PDF of reflectivities computed for rain below the melting level, where rain is the only precipitation type, shows large values (often larger than 10 km). Even higher values of z_0 found for rain above 6 km are coming from infrequent, but highly vertically coherent, active convective cores. Correlation length scale for snow is on the order of 1 km. The vertical profile of z_0 for graupel is similar to that of rain (above the melting level), but with slightly lower values.

3.2. Model Simulations

Figure 9 shows z_0 for ranked correlation coefficients computed for PDFs of model-predicted hydrometeor mass mixing ratios at two adjacent levels. Unlike Ovchinnikov et al. (2016), who analyzed the behavior of z_0 profiles over selected 24-hr periods, here z_0 evolution is presented for the entire simulations, although the main features of the mean profiles remain the same. These include larger z_0 (i.e., stronger PDF correlations) for rain and graupel compared to snow, which is especially evident in the SGP simulation, and a significantly different PDF correlation for rain mixing ratio above and below the melting level.

While there are obvious similarities between profiles of z_0 for radar-measured reflectivity (Figure 8) and model-predicted mixing ratio (Figure 9), there are also notable differences. Many of these differences stem from the fact that although rain, snow, and graupel are used as hydrometeor categories in both observations and model simulations, there is no one-to-one correspondence between them. First, observed and modeled variables represent different properties of hydrometeors, that is, reflectivity factor versus mass mixing ratio. (Modeled number mixing ratios are also analyzed, but not shown here). Since these properties are affected by physical processes with different spatial distributions, their overlap characteristics are expected to vary as well. The second important distinction, already mentioned above, is that radar-based classification assigns a single hydrometeor type to each location, while in the model representation hydrometeors of several types can coexist at the same location. As a result, extension of profiles of z_0 for snow and graupel below the melting level and low z_0 values for rain above the melting level seen in the model results (Figure 9) may not appear in observational analysis (Figure 8) because the corresponding hydrometeors are usually not of dominant type at these levels.

3.3. Correlation Length Scale as a Function of Fall Speed

Results presented above and earlier in Ovchinnikov et al. (2016) point to the fall speed as one of the primary factors controlling the PDF overlap, as measured by the correlation length scale z_0. Here, we seek to quantify the z_0—fall speed relationship in a way that can be used in a parameterization of PDF correlation in large-scale models.

Scatter plots of z_0 from Figures 8 and 9 versus fall speeds from Figures 3 and 7 are shown in Figure 10. Model results panels also include corresponding parameters for cloud ice mass and number mixing ratios for all model hydrometeor types, which are not shown in earlier figures. In addition, z_0 for cloud liquid water mass and number mixing ratios are also computed and used in the analysis, including linear fitting discussed later.

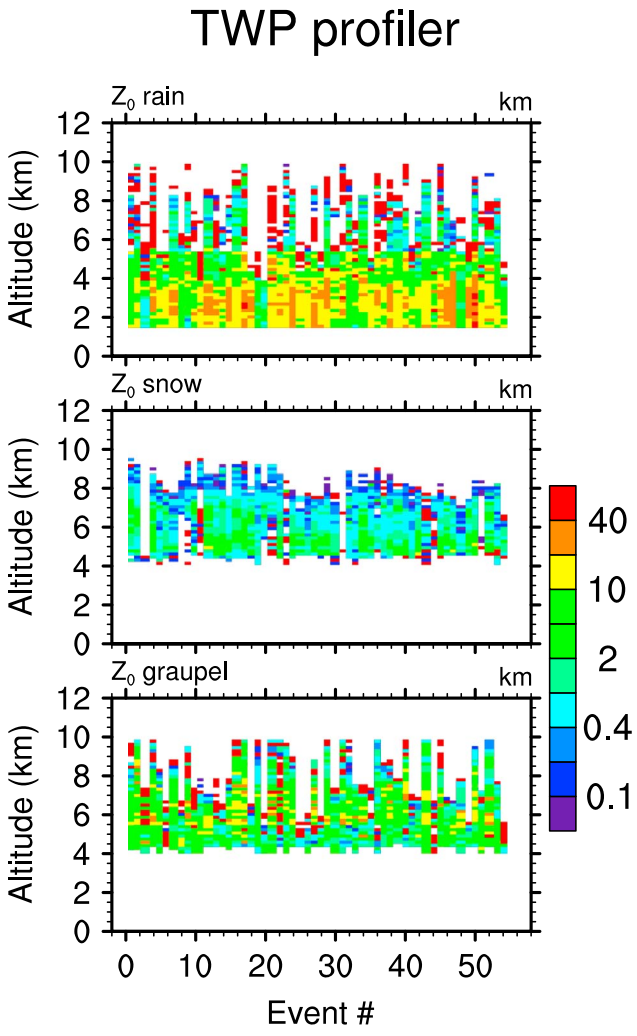

Figure 8. Profiles of vertical correlation length scale (z_0, km) for radar reflectivity probability density functions for 54 events. Correlations are computed for probability density functions of radar reflectivity factor at two neighboring levels 100 m apart as described in the text. Panels from top to bottom are for rain, snow, and graupel, respectively. TWP = Tropical Warm Pool.

These points are not shown in Figures 10a–10c, however, because they have zero fall speed, which is not displayable on a logarithmic axis. Although points are spread over 2 orders of magnitude ranges along both axes, there is a clear trend for increasing z_0 with increasing fall speed. The overall correlation is moderate with linear correlation coefficients between z_0 and fall speed calculated for SGP model, TWP model, and TWP radar profiler are found to be of 0.62, 0.58, and 0.61, respectively. By examining the relationship separately for each microphysical variable or hydrometeor class, which are color coded in Figure 10, we see that the overall dependency is driven primarily by systematic differences among these hydrometeor types. Indeed, each category occupies a relative narrow fall speed band but contains a wide range of z_0 values, resulting in low to no correlation between z_0 and fall speed within each species. This is common for nearly all modeled and observationally diagnosed categories, except for modeled rain, which shows correlations above 0.5 for both number and mass mixing ratios in both simulated cases.

Figure 11 summarizes z_0—fall speed relationship. Here each point represents average z_0 and fall speed for one microphysical class (variable) for a particular simulation or observational data set. It must be noted that averaging is performed for rank correlations, rather than correlation length scales. This is because the two variables have a highly nonlinear relationship between them (see equation (1)), with the rank correlation being the relevant quantity for drawing subcolumn samples from PDFs. Direct averaging of z_0 would lead to a correlation estimate that is biased high. To mitigate the effect of different layer separation distances, all rank correlations (R) are converted to a nominal $\Delta z = 100$ m using (1) before averaging. Once the mean rank correlations for all species are computed, they are converted, again using (1), back into mean length scales plotted in Figure 11. Fall speeds are weighted by the corresponding property, that is, number or mass mixing ratio, or radar reflectivity, when averages are computed. We also use area fractional cover weighting in computing time and altitude averages for both z_0 and fall speed. A logarithmic scale is chosen for the fall speed axis to better distinguish several slowly falling species. Consequently, zero fall speeds for cloud mass and number mixing ratios cannot be plotted on that axis and their corresponding z_0 values are indicated by horizontal dashed lines color coded by simulated cases as are the other model species. The plot confirms a strong positive covariance of the correlation length scale and fall speed. A linear regression in the form

$$z_0 = a + bV_f \tag{2}$$

with $a = 0.69$ and $b = 0.67$ for V_f in meters per second and z_0 in kilometers provides a correlation coefficient of 0.80 (Figure 11). All 23 data points are used in the fit: number and mass mixing ratios for five hydrometeor classes (cloud liquid, cloud ice, rain, snow, and graupel) for two simulations (SGP and TWP) and three points for radar reflectivity for rain, snow, and graupel. A nearly identical quality fit is also obtained with a power law function in the form

$$z_0 = a_p + b_p V_f^{c_p} \tag{3}$$

where $a_p = 0.38$, $b_p = 1.18$, and $c_p = 0.73$.

3.4. Correlation Length Scale Dependence on Wind Shear

When the horizontal wind changes with altitude, distributions of species at different levels shift relative to each other and therefore become less correlated. To examine this effect, we plot z_0 computed from the

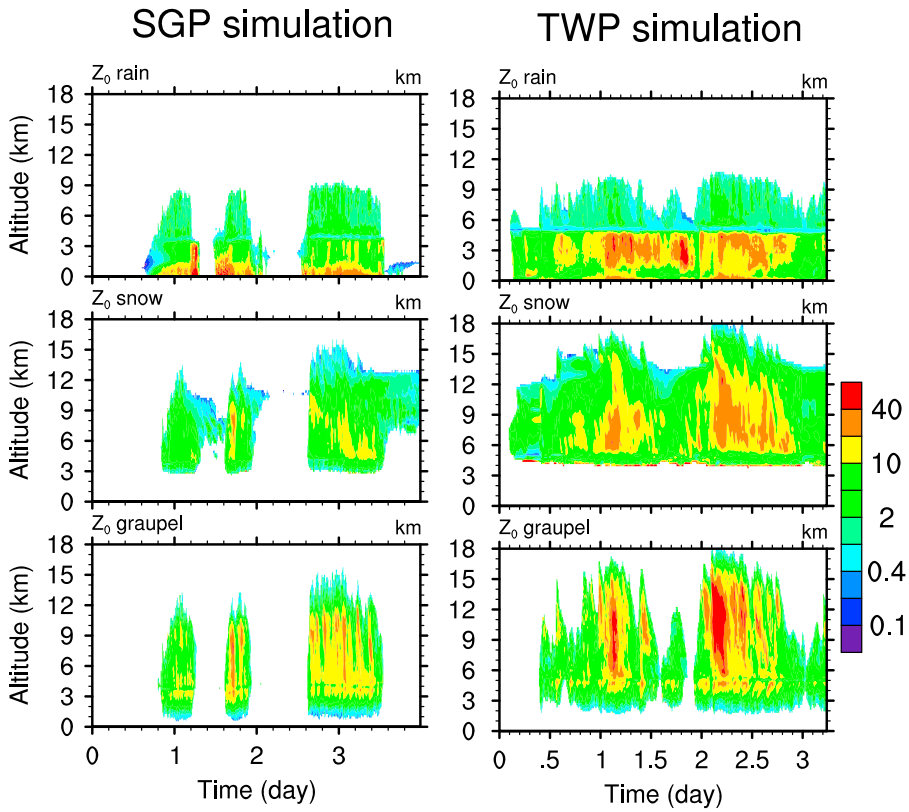

Figure 9. Time evolution of the profiles of vertical correlation length scale (z_0, km) for mass mixing ratio probability density functions for Soithern Great Plains (SGP, left column) and Tropical Warm Pool (TWP, right column) simulations. Panels from top to bottom are for rain, snow, and graupel, respectively.

rank correlation of species distribution at two levels against the mean wind shear between these levels (Figures 10d–10f). The wind shear strength is defined here as the absolute value of the vector difference of horizontal wind at the two levels divided by the vertical distance between these levels. Such defined wind shear includes the effects of changes in horizontal wind strength, as well as direction. Observed horizontal wind components are taken from the 50-MHz wind profiler on the day of an observed convective event. For simulations, wind shear is computed from domain mean profiles of horizontal wind components. Although the wind shear is expected to reduce the vertical coherency of horizontal distributions, we find that z_0 and wind shear are virtually uncorrelated (Figures 10d–10f), with correlation coefficients of 0.16, 0.13, and 0 calculated for SGP model, TWP model, and TWP radar profiler, respectively. This is because large systematic differences in vertical overlap among various species discussed earlier drive much of the overall variability in z_0 making it independent of the wind shear. Analyzing individual species separately, thereby constraining z_0 variability to narrower ranges, the effect of wind shear becomes more pronounced, at least in simulation results. Most modeled species exhibit some negative correlation between z_0 and wind shear, as expected, with generally stronger negative correlation for species with slower fall speeds, that is, cloud liquid droplet and ice crystals (Figures 10d–10f). An exception to that rule is a positive correlation between z_0 and wind shear for rain properties, especially in the case of continental convection (SGP, Figure 10d). This positive correlation stems from a relatively small number of instances when vertically coherent rain shafts with high z_0 values go through a relatively shallow layer with strongest wind shear values at the top of the boundary layer.

4. Discussion

The PDF overlap considered here provides a measure of vertical coherence, or vertical alignment, of horizontal inhomogeneities of clouds and precipitation. Vertical PDF overlap, or, more generally, the three-

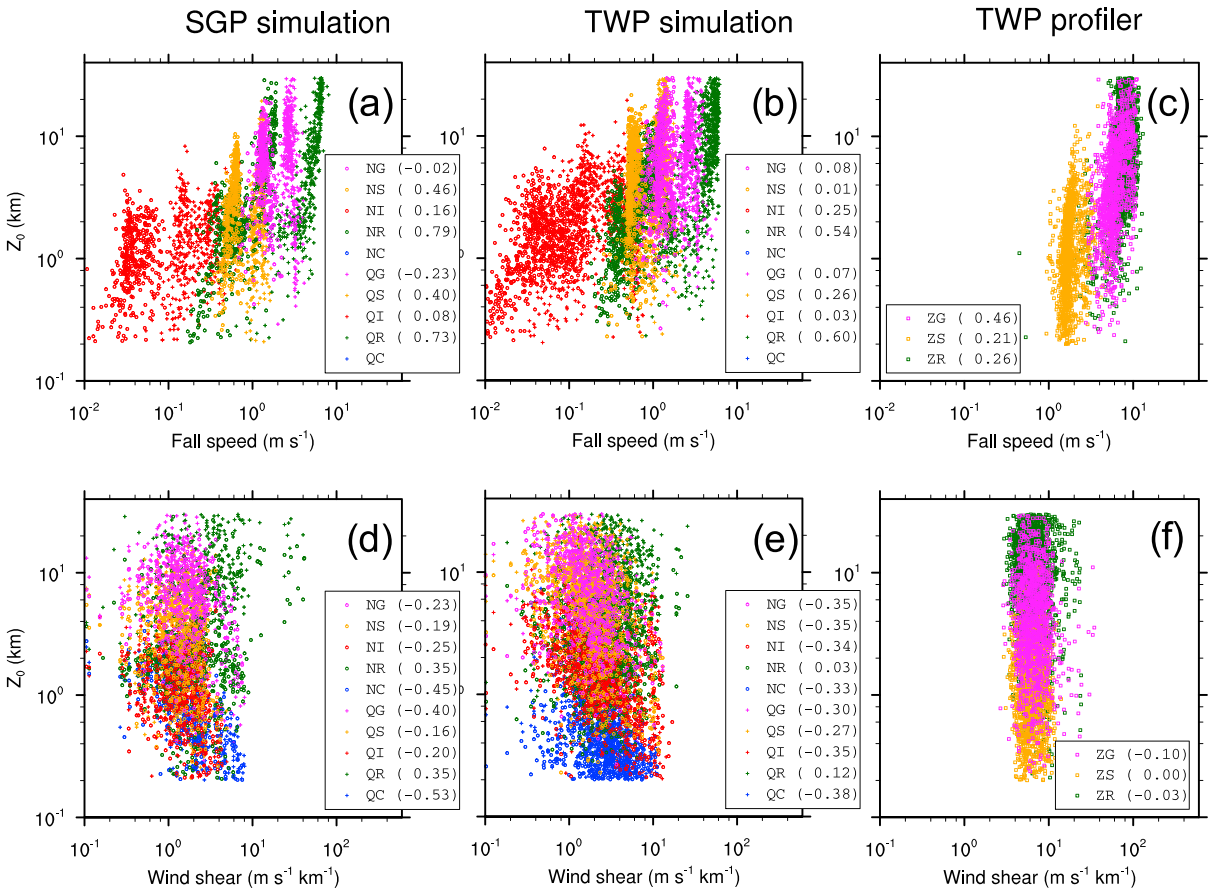

Figure 10. Dependency of the probability density function correlation length scale (z_0) on fall speed (a–c) and wind shear (d–f) for model predicted number and mass mixing ratios and observed radar reflectivity factor for three hydrometeor classes (rain, snow, and graupel), as indicated by the legend on each panel. Linear correlation coefficients for each of the shown microphysical species are also given in the legends next to a variable name. Cloud droplet number and mass mixing ratios (NC and QC) are also included on panels (d) and (e) but are omitted from panels (a) and (b) because these species have zero fall speeds. For model simulations, only every 25th point is shown to improve the readability of the figures. SGP = Southern Great Plains; TWP = Tropical Warm Pool.

dimensional spatial distribution of microphysical variables, is affected by four categories of processes: spatial and temporal heterogeneity of sources and sinks, transport of hydrometeors by vertical air motions, transport (advection) of hydrometeors by horizontal air motions, and sedimentation of hydrometeors to lower levels. For instance, higher correlation results when certain species are generated within vertically coherent structures, such as convective towers and/or transported between layers by vertical air motions (updrafts or downdrafts). Higher correlation also results from rapid sedimentation. Wind shear reduces the vertical correlation because it disrupts interlayer coupling by tilting updrafts, downdrafts, and trajectories of falling hydrometeors.

Several attempts to characterize wind shear effects have been made recently. Di Giuseppe and Tompkins (2015) used overlapping clouds observed by CloudSat and wind fields from ECMWF reanalysis to construct a parameterization that reduces correlation length scale with increasing wind shear. Li et al. (2018) also used CloudSat-derived cloud geometry and ERA-Interim reanalysis to quantify dependence of correlation length scale on wind shear. Both studies propose a linear decrease in the correlation length scale with wind shear, although the strength of the relationship given by the slope parameter varies by as much as a factor of 5 from $z_0 = 4.4–0.45\ dU/dz$ in Di Giuseppe and Tompkins (2015) to $z_0 = 2.19–0.09\ dU/dz$ in Li et al. (2018). It is important to keep in mind that these studies deal with cloud occurrence, or cloud fraction, overlap, not PDF overlap considered here, but if the strength of the wind shear effect on PDF overlap were comparable to these estimates, it appears that the effect of the fall speed would still dominate because the V_f prefactor in

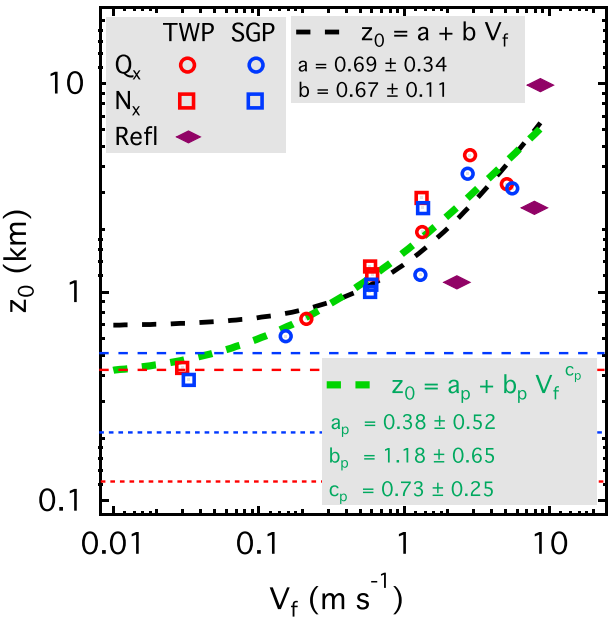

Figure 11. Mean vertical probability density function correlation length scale (z_0) versus mean fall speed (V_f) for simulated and observed cloud and precipitation properties. Model properties include mass (circles, Q_x) and number (squares, N_x) mixing ratios for rain, cloud ice, snow, and graupel for Soithern Great Plains (SGP, blue) and Tropical Warm Pool (TWP, red) cases. The parameter z_0 for nonprecipitating cloud water mass and number mixing ratios, that is, species with zero fall speeds, are indicated by horizontal long and short dashed lines, respectively. Diamonds mark z_0 for radar reflectivity and associated fall speed for rain, snow, and graupel. The best linear and power law fits are shown by thick black and green dashed lines, respectively. Coefficients of these fits plus and minus their standard deviations are also shown in the inserts.

equation (2) is significantly larger than the dU/dz prefactors given above, while the range of variations in fall speed (0 to 8 m/s) is comparable to that of the wind shear (0 to 6 $m{\cdot}s^{-1}{\cdot}km^{-1}$).

Figure 11 suggests that z_0 can be expressed as varying approximately linearly with V_f. When we perform a power law fit, we obtain an exponent of 0.73 ± 0.25, which indicates a dependency between linear and square root. To rationalize the functional form of the found empirical relationship, we consider the following idealized example involving evaporation of rain. Suppose that a layer aloft has a continuous source of a hydrometeor species. For concreteness, suppose that the melting of snow generates rain at the melting level. The source creates a layer with a horizontally inhomogeneous distribution. Now suppose that the rain drops fall from the melting level with a mean speed of V_f. Further suppose that falling rain is subjected to a process with a horizontally inhomogeneous process rate, such as inhomogeneous evaporation, which acts to change the rank ordering of the parcels with time. After a time τ, the rank correlation with the source layer aloft has changed by e^{-1}. At this time, the rain will have fallen a distance z_0, by definition and, therefore, $z_0 = V_f\,\tau$. We see that τ represents a time scale over which the rank correlation is changed significantly by a process such as evaporation, or sublimation. Being defined by the microphysical process, the decorrelation time τ can be independent of z_0 and V_f, in which case z_0 becomes proportional to V_f. This conceptual framework illustrated in Figure 12a should not be taken too literally because it ignores factors such as size sorting of hydrometeors and time variations of the source aloft. However, the framework does help clarify the nature of the decorrelation time, τ, and its influence on the form of the z_0-V_f relationship.

Now consider a second example in which vertical wind shear rather than evaporation or another microphysical process is the cause of vertical decorrelation. Namely, consider an idealized situation in which precipitation from a continuous-in-time horizontally inhomogeneous source at one level falls with a mean fall speed V_f through a layer with a constant wind shear (dU/dz). In this example, we assume that the horizontal distributions (or, at least, their rank distributions) of precipitation at any altitude below the source level are identical except for the horizontal shift. The fields at two levels separated by z_0 are shifted relative to each other at a rate of $\Delta U = (dU/dz)z_0$ (Figure 12b). In the time that it takes precipitation to fall the distance z_0 with the fall speed V_f, the two fields must be shifted by a distance equal to the horizontal correlation length scale L (the same for all levels under the described example). That is, by definition, two layers separated vertically by z_0 have a rank correlation of e^{-1} and that degree of decorrelation is achieved by shifting the layer horizontally by a distance L. Equating the time for the horizontal shift over the distance L with the time for the fall over the distance z_0, we obtain $L/\Delta U = z_0/V_f$, which, after substituting the above expression for ΔU and rearranging, yields $z_0^2 = LV_f/(dU/dz)$. Although admittedly simplistic, this conceptual model suggests that if vertical decorrelation is driven by the horizontal wind-shear-induced shift of layers falling from a horizontally inhomogeneous source, then proportionality of z_0 to the square root of the fall speed should be expected. Note that this would only be the case if all involved parameters are independent of each other. If, for example, z_0 is proportional to L, then we see that once again z_0 goes as V_f to the power of 1.

Looking back at the z_0-V_f relationship expressed in the form of a power law (equation (3)), we note that the best fit exponent is between 0.5 and 1, which are the values derived from the two idealized examples described above. Hence, it is possible that although the wind shear is not explicitly accounted for in this expression, its effect is manifested indirectly through the reduction of the V_f exponent. Further investigation into the relationship between z_0 and horizontal decorrelation length scale, fall speed, and wind shear is clearly needed.

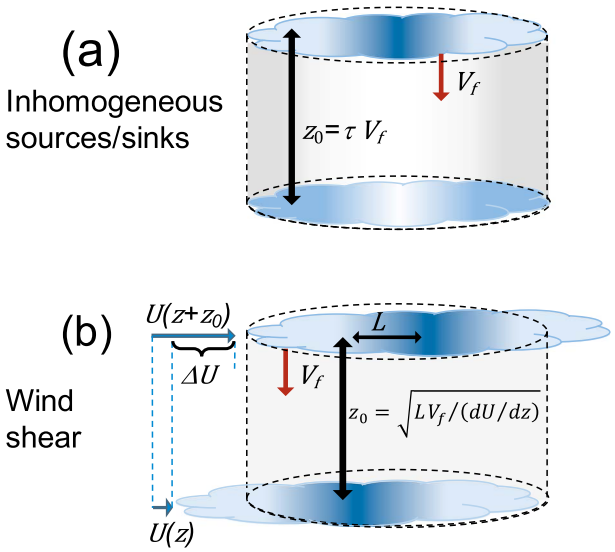

Figure 12. Illustrations of two conceptual mechanisms for sedimentation to affect a rank correlation of a species distributions at two levels: (a) Horizontally inhomogeneous environment altering the ranking of parcels in a layer falling with speed of V_f through a process, such as evaporation, that reduces the rank correlation by a factor of e^{-1} in time τ. (b) A layer with a horizontal correlation length scale L is falling with a speed V_f while experiencing a horizontal shift due to vertical wind shear (dU/dz). See text for more details.

5. Summary

This study aims to improve the representation of vertical alignment of cloud and precipitation properties that vary horizontally on a subgrid scale in climate models. For processes, for example, radiation transfer and for diagnostics, for example, satellite instrument simulators, for which the vertical structure of these fields is important, distributions, or PDFs, of these variables within each model grid cell must be linked in the vertical using appropriate overlap assumptions. The degree of PDF overlap is characterized here using rank correlation of variable distributions at two levels. The dependence of the rank correlation on the layer separation is mitigated by computing a correlation length scale, defined as a distance over which the rank correlation drops by a factor of e^{-1}, assuming exponential decay of correlation with increasing distance between the layers. This study builds on the work by Ovchinnikov et al. (2016), who found that the vertical overlap for PDFs of different properties (i.e., number and mass mixing ratios) and different hydrometeor types (i.e., cloud liquid and ice, rain, snow, and graupel) varies widely and suggested that corresponding fall speed might be the primary factor controlling the degree of their vertical alignment. Here, we quantify the relationship between the length scale z_0 for the correlation between PDFs of a cloud or precipitation property at two levels and the mean fall speed V_f for that property using cloud-resolving model (CRM) simulations and radar profiler observations. Model output is taken from two multiday simulations of convection under midlatitude continental and tropical oceanic convection. Vertical correlation length scale and fall speed are analyzed for a number of variables or species, including model predicted microphysics variables (number and mass mixing ratios for cloud liquid and ice, rain, snow, and graupel) and for reflectivity factors observed by the vertically pointing dual-frequency radar profilers near Darwin, Australia, from November 2005 to April 2006. Each z_0 and V_f profile corresponds to either an instantaneous snapshot of a 3-D model-generated field or a day-long height-time data set from the profilers. When these quantities for each species are averaged over altitude and time, a well-defined correlation between z_0 and V_f emerges (Figure 11). Both linear and power law functional forms provide comparable fits to the found dependency.

Although it is clear that a number of factors can affect the vertical overlap of PDFs of various cloud and precipitation properties, the presented study demonstrates that effective fall speed associated with these properties accounts for the majority of variation in their mean correlation length scale. A simple linear fit exhibits a high linear correlation coefficient of 0.8 (Figure 11). This fit covers a wide range of fall speeds, from 0 to over 7 m/s, and therefore should be applicable to most microphysics variables used in large-scale models. Given that each point on that plot represents an average over many times, altitudes, and different cloud populations, the relationship must be viewed as statistical, but so is the PDF representation of subgrid variability of microphysics variables. For each hydrometeor class, z_0 varies significantly about the mean (Figures 10), often with no or weak correlation with V_f. One of the main sources of these variations is height dependencies of both z_0 and fall speed (Figures 3, and 7–9). It might be possible to incorporate altitude (or temperature) explicitly into a parametric representation of z_0, but such a correction will necessarily be dependent on pre-defined classes of hydrometeors, making such a parameterization microphysics specific. For example, based on numerical simulations of tropical maritime convection, Wang (2017) proposed to parameterize z_0 for cloud liquid and ice water content as a piecewise linear function of pressure, with smaller values near the surface (0.6 km) and tropopause (0.5 km) and larger values (2.3 km) in the midtroposphere. That study used SAM model with a one-moment microphysics, in which cloud water diagnosed from the prognostic total water variable is partitioned into liquid and ice using a simple temperature-dependent formulation. Using the same model (SAM) with a more elaborate two-moment microphysics, we find qualitatively similar z_0 profiles for cloud liquid and ice water, but significantly different profiles for rain and other precipitating species (see also Ovchinnikov et al., 2016). Thus, additional studies are needed to find a more general way to represent variation of z_0 with altitude.

It is worth emphasizing that the proposed parameterization of the vertical PDF overlap is based on a physical property (i.e., fall speed) of hydrometeors rather than artificially defined and model-specific hydrometeor types. As such, it can be applied to a wide range of microphysics representations in regional and global models, including not only traditional schemes with pre-defined discrete ice categories, such as cloud ice, snow, and graupel, but also emerging treatments using a continuous representation of solid hydrometeors, for example, the Predicted Particle Properties (P3; Morrison & Milbrandt, 2015) or Ice-Spheroids Habit Model with Aspect-Ratio Evolution (ISHMAEL; Jensen et al., 2017) schemes.

Several recent studies attempted to rationalize and quantify the dependency of a cloud fraction overlap parameter on the horizontal scale of the cloud scene used to derive it (e.g., Astin & Di Girolamo, 2014; Tompkins & Di Giuseppe, 2015). The PDF overlap examined here is also likely to exhibit a scale dependency, as suggested by Hogan and Illingworth (2003). Such a dependency could be important to take into account in developing parameterizations suitable for models of different horizontal resolutions. In the presented study, the horizontal extent of the simulation domain is on the order of 100×100 km^2, which makes the result most directly applicable to the global model grid size approximately $1° \times 1°$. It is difficult to define a horizontal scale for a day-long data set of radar profiles because of the involved time evolution and wind variability in height (see, e.g., Boutle et al., 2014), but a horizontal wind of few meters per second translates into hundreds of kilometers over the course of the day. Analyzing model subdomains of various sizes and sampling periods of different lengths in future studies will be useful in adressing the scale dependency of the PDF overlap and its relationships with hydrometeor fall speeds and wind shear.

Acknowledgments
This research was supported by the Climate Model Development and Validation activity funded by the Office of Biological and Environmental Research in the U.S. Department of Energy Office of Science, with V. Larson's portion supplied by grant DE-SC0016287. The Pacific Northwest National Laboratory (PNNL) is operated for DOE by Battelle Memorial Institute under contract DE-AC05-76RLO1830. The SAM model is available from Marat Khairoutdinov of Stony Brook University at http://rossby.msrc.sunysb.edu/~marat/SAM.html website. Forcing data are available from the ARM program archive, sponsored by the DOE Office of Science. Computing resources for the simulations were provided by the National Energy Research Scientific Computing Center (NERSC).

References

Astin, I., & Di Girolamo, L. (2014). Technical note: The horizontal scale dependence of the cloud overlap parameter α. *Atmospheric Chemistry and Physics*, *14*(18), 9917–9922. https://doi.org/10.5194/acp-14-9917-2014

Barker, H. W. (2008). Overlap of fractional cloud for radiation calculations in GCMs: A global analysis using CloudSat and CALIPSO data. *Journal of Geophysical Research*, *113*, 15, D00A01. https://doi.org/10.1029/2007jd009677

Bodas-Salcedo, A., Webb, M. J., Bony, S., Chepfer, H., Dufresne, J. L., Klein, S. A., et al. (2011). COSP satellite simulation software for model assessment. *Bulletin of the American Meteorological Society*, *92*(8), 1023–1043. https://doi.org/10.1175/2011bams2856.1

Boutle, I. A., Abel, S. J., Hill, P. G., & Morcrette, C. J. (2014). Spatial variability of liquid cloud and rain: Observations and microphysical effects. *Quarterly Journal of the Royal Meteorological Society*, *140*(679), 583–594. https://doi.org/10.1002/qj.2140

Di Giuseppe, F., & Tompkins, A. M. (2015). Generalizing cloud overlap treatment to include the effect of wind shear. *Journal of the Atmospheric Sciences*, *72*(8), 2865–2876. https://doi.org/10.1175/jas-d-14-0277.1

Giangrande, S. E., Collis, S., Straka, J., Protat, A., Williams, C., & Krueger, S. (2013). A summary of convective-core vertical velocity properties using ARM UHF wind profilers in Oklahoma. *Journal of Applied Meteorology and Climatology*, *52*(10), 2278–2295. https://doi.org/10.1175/jamc-d-12-0185.1

Giangrande, S. E., Toto, T., Jensen, M. P., Bartholomew, M. J., Feng, Z., Protat, A., et al. (2016). Convective cloud vertical velocity and mass-flux characteristics from radar wind profiler observations during GoAmazon2014/5. *Journal of Geophysical Research: Atmospheres*, *121*, 12,891–12,913. https://doi.org/10.1002/2016jd025303

Griffin, B. M., & L, V. E. (2016). Parameterizing microphysical effects on variances and covariances of moisture and heat content using a multivariate probability density function: A study with CLUBB (tag MVCS). *Geoscientific Model Development*, *9*(11), 4273–4295. https://doi.org/10.5194/gmd-9-4273-2016

Hillman, B. R., Marchand, R. T., & Ackerman, T. P. (2018). Sensitivities of simulated satellite views of clouds to subgrid-scale overlap and condensate heterogeneity. *Journal of Geophysical Research: Atmospheres*, *123*, 7506–7529. https://doi.org/10.1029/2017JD027680

Hogan, R. J., & Illingworth, A. J. (2003). Parameterizing ice cloud inhomogeneity and the overlap of inhomogeneities using cloud radar data. *Journal of the Atmospheric Sciences*, *60*(5), 756–767. https://doi.org/10.1175/1520-0469(2003)060<0756:piciat>2.0.co;2

Jensen, A. A., Harrington, J. Y., Morrison, H., & Milbrandt, J. A. (2017). Predicting ice shape evolution in a bulk microphysics model. *Journal of the Atmospheric Sciences*, *74*(6), 2081–2104. https://doi.org/10.1175/jas-d-16-0350.1

Khairoutdinov, M., & Randall, D. (2003). Cloud resolving modeling of the ARM summer 1997 IOP: Model formulation, results, uncertainties, and sensitivities. *Journal of the Atmospheric Sciences*, *60*(4), 607–625. https://doi.org/10.1175/1520-0469(2003)060<0607:CRMOTA>2.0.CO;2

Kumar, V. V., Jakob, C., Protat, A., Williams, C. R., & May, P. T. (2015). Mass-flux characteristics of tropical cumulus clouds from wind profiler observations at Darwin, Australia. *Journal of the Atmospheric Sciences*, *72*(5), 1837–1855. https://doi.org/10.1175/jas-d-14-0259.1

Larson, V. E. (2007). From cloud overlap to PDF overlap. *Quarterly Journal of the Royal Meteorological Society*, *133*(628), 1877–1891. https://doi.org/10.1002/qj.165

Li, J., Lv, Q., Jian, B., Zhang, M., Zhao, C., Fu, Q., et al. (2018). The impact of atmospheric stability and wind shear on vertical cloud overlap over the Tibetan plateau. *Atmospheric Chemistry and Physics*, *18*(10), 7329–7343. https://doi.org/10.5194/acp-18-7329-2018

Marchand, R. (2012). Spatial correlation of hydrometeor occurrence, reflectivity, and rain rate from CloudSat. *Journal of Geophysical Research*, *117*, D06202. https://doi.org/10.1029/2011jd016678

May, P. T., Mather, J. H., Vaughan, G., Jakob, C., McFarquhar, G. M., Bower, K. N., & Mace, G. G. (2008). The tropical warm pool international cloud experiment. *Bulletin of the American Meteorological Society*, *89*(5), 629–645. https://doi.org/10.1175/bams-89-5-629

Morrison, H., Curry, J. A., & Khvorostyanov, V. I. (2005). A new double-moment microphysics parameterization for application in cloud and climate models. Part I: Description. *Journal of the Atmospheric Sciences*, *62*(6), 1665–1677. https://doi.org/10.1175/JAS3446.1

Morrison, H., & Milbrandt, J. A. (2015). Parameterization of cloud microphysics based on the prediction of bulk ice particle properties. Part I: Scheme description and idealized tests. *Journal of the Atmospheric Sciences*, *72*(1), 287–311. https://doi.org/10.1175/jas-d-14-0065.1

Morrison, H., Thompson, G., & Tatarskii, V. (2009). Impact of cloud microphysics on the development of trailing stratiform precipitation in a simulated squall line: Comparison of one- and two-moment schemes. *Monthly Weather Review*, *137*(3), 991–1007. https://doi.org/10.1175/2008mwr2556.1

Neggers, R. A. J., Heus, T., & Siebesma, A. P. (2011). Overlap statistics of cumuliform boundary-layer cloud fields in large-eddy simulations. *Journal of Geophysical Research*, *116*, D21202. https://doi.org/10.1029/2011jd015650

North, K. W., Oue, M., Kollias, P., Giangrande, S. E., Collis, S. M., & Potvin, C. K. (2017). Vertical air motion retrievals in deep convective clouds using the ARM scanning radar network in Oklahoma during MC3E. *Atmospheric Measurement Techniques*, *10*(8), 2785–2806. https://doi.org/10.5194/amt-10-2785-2017

Oreopoulos, L., Chou, M. D., Khairoutdinov, M., Barker, H. W., & Cahalan, R. F. (2004). Performance of Goddard Earth observing system GCM column radiation models under heterogeneous cloud conditions. *Atmospheric Research*, *72*(1–4), 365–382. https://doi.org/10.1016/j.atmosres.2004.03.025

Ovchinnikov, M., Lim, K. S. S., Larson, V. E., Wong, M., Thayer-Calder, K., & Ghan, S. J. (2016). Vertical overlap of probability density functions of cloud and precipitation hydrometeors. *Journal of Geophysical Research: Atmospheres*, *121*, 12,966–12,984. https://doi.org/10.1002/2016jd025158

Paquin-Ricard, D., Vaillancourt, P. A., Barker, H. W., & Cole, J. N. S. (2016). A comparison of two representations of subgrid-scale cloud structure in a global model: Radiative effects as a function of cloud characteristics. *Quarterly Journal of the Royal Meteorological Society*, *142*(699), 2551–2561. https://doi.org/10.1002/qj.2846

Pincus, R., Hannay, C., Klein, S. A., Xu, K. M., & Hemler, R. (2005). Overlap assumptions for assumed probability distribution function cloud schemes in large-scale models. *Journal of Geophysical Research*, *110*, D15S09. https://doi.org/10.1029/2004jd005100

Protat, A., & Williams, C. R. (2011). The accuracy of radar estimates of ice terminal fall speed from vertically pointing Doppler radar measurements. *Journal of Applied Meteorology and Climatology*, *50*(10), 2120–2138. https://doi.org/10.1175/jamc-d-10-05031.1

Raisanen, P., Barker, H. W., Khairoutdinov, M. F., Li, J. N., & Randall, D. A. (2004). Stochastic generation of subgrid-scale cloudy columns for large-scale models. *Quarterly Journal of the Royal Meteorological Society*, *130*(601), 2047–2067. https://doi.org/10.1256/qj.03.99

Schumacher, C., Stevenson, S. N., & Williams, C. R. (2015). Vertical motions of the tropical convective cloud spectrum over Darwin, Australia. *Quarterly Journal of the Royal Meteorological Society*, *141*(691), 2277–2288. https://doi.org/10.1002/qj.2520

Tompkins, A. M., & Di Giuseppe, F. (2015). An interpretation of cloud overlap statistics. *Journal of the Atmospheric Sciences*, *72*(8), 2877–2889. https://doi.org/10.1175/jas-d-14-0278.1

Wang, X. C. (2017). Effects of cloud condensate vertical alignment on radiative transfer calculations in deep convective regions. *Atmospheric Research*, *186*, 107–115. https://doi.org/10.1016/j.atmosres.2016.11.014

Williams, C. R. (2012). Vertical air motion retrieved from dual-frequency profiler observations. *Journal of Atmospheric and Oceanic Technology*, *29*(10), 1471–1480. https://doi.org/10.1175/jtech-d-11-00176.1

Wong, M., & Ovchinnikov, M. (2017). PDF-based parameterization of subgrid-scale hydrometeor transport in deep convection. *Journal of the Atmospheric Sciences*, *74*(4), 1293–1309. https://doi.org/10.1175/jas-d-16-0146.1

Wong, M., Ovchinnikov, M., & Wang, M. H. (2015). Evaluation of subgrid-scale hydrometeor transport schemes using a high-resolution cloud-resolving model. *Journal of the Atmospheric Sciences*, *72*(9), 3715–3731. https://doi.org/10.1175/jas-d-15-0060.1

Xu, K. M., Cederwall, R. T., Donner, L. J., Grabowski, W. W., Guichard, F., Johnson, D. E., et al. (2002). An intercomparison of cloud-resolving models with the atmospheric radiation measurement summer 1997 intensive observation period data. *Quarterly Journal of the Royal Meteorological Society*, *128*(580), 593–624. https://doi.org/10.1256/003590002321042117